energies

MDPI

Article

Study on Erosion Model Optimization and Damage Law of Coiled Tubing

Binqi Zhang [1,2], Jingen Deng [1,*], Hai Lin [2], Jie Xu [2], Guiping Wang [2], Wei Yan [1], Kongyang Wang [2] and Fuli Li [1]

[1] State Key Laboratory of Oil and Gas Resources and Detection, China University of Petroleum, Beijing 102249, China
[2] Tianjin Branch, CNOOC (China) Co., Ltd., Tianjin 300459, China
* Correspondence: dengjg@cup.edu.cn

Abstract: Coiled tubing (CT) is used as a velocity string to transport high-velocity gas in drainage gas recovery technology. Sand particles flowing at high speed can cause serious erosion of the pipe wall. Long-term erosion wear leads to the degradation of the string strength and can even cause local perforation. In order to study the erosion wear problem of CT, a gas–solid erosion experimental device was established for a full-size pipe with different radii of curvature. A 3D laser confocal technique was used to examine and characterize the microscopic erosion morphology of the inner wall of the CT. The CFD erosion model was selected based on the erosion test data of the inner wall of the CT, and the erosion results of the Finnie model show minimal error and good agreement compared with other models. The average value of the error of the maximum erosion rate at different radii of curvature is 8.3%. The effect of the radius of curvature, gas velocity and solid particle size on the maximum erosion rate of the inner wall of the CT was analyzed based on the Finnie model. The results reveal that erosion wear occurs on the inner wall of the CT's outer bend. As the radius of curvature is reduced, the maximum erosion rate and area increase, and the position of the maximum erosion rate gradually shifts toward the inlet. The maximum erosion rate is positively correlated with the gas flow rate. However, as the particle size increases, the maximum erosion rate shows a trend of first increasing, then decreasing and finally stabilizing, with a critical particle size of 200 μm. This study can provide theoretical guidance and methods for improving the service life of CT. The erosion rate of the tubing in old wells can be reduced by controlling production and employing appropriate sand control methods, while the erosion rate of tubing in new wells can be reduced by adjusting the wellbore trajectory.

Keywords: coiled tubing; erosion wear; model optimization; damage law; high-producing gas well

Citation: Zhang, B.; Deng, J.; Lin, H.; Xu, J.; Wang, G.; Yan, W.; Wang, K.; Li, F. Study on Erosion Model Optimization and Damage Law of Coiled Tubing. *Energies* **2023**, *16*, 2775. https://doi.org/10.3390/en16062775

Academic Editor: Reza Rezaee

Received: 17 February 2023
Revised: 11 March 2023
Accepted: 14 March 2023
Published: 16 March 2023

1. Introduction

Coiled tubing has been widely used in oil and gas field operations due to its small footprint, low operating cost and wide range of applications, solving many problems that are difficult to overcome with conventional operating techniques. The solid-phase particles carried by the fluid can cause severe erosion and wear to the pipe wall when transporting high-flow-rate gas as a production string in drainage gas production technology [1,2]. Therefore, it is important to reveal the erosion mechanism of gas and solid-phase flow in CT and clarify the maximum erosion rate of the CT and the area where it is located in order to prolong and improve the effective service life of CT.

In the process of exploring the mechanism of erosion wear, many scholars have achieved promising results. Reynolds [3] and Rayleigh [4] summarized the phenomenon of erosion and wear and put forward a theory of erosion for the first time. In 1958, Finnie [5] put forward a theory of erosion of plastic materials and established an erosion model for the first time in 1960, which laid the foundation for the development of subsequent erosion models. Erosion is a very complex process influenced by many factors. Although

empirical or semiempirical erosion models based on various influencing factors have been proposed by many scholars through experiments [6–12], due to the complexity of erosion mechanisms and differences in experimental conditions, the application conditions of different types of erosion models are limited, which may lead to uncertainties when used under a wider range of conditions [13]. With the development of computational fluid dynamics (CFD) technology, numerical simulation has become an important way to study the erosion and wear of pipes. In 2001, Edwards [14] et al. developed a CFD model to simulate the erosion rate of pipes for the erosion of two-phase flow at elbows and proposed a new method to study the erosion of gas–solid two-phase flow. Shah [15] et al. studied the influence of erosion in coiled tubing using the CFD technique and concluded that flow rate is the most important factor affecting erosion. Pandya [16] et al. proposed an improved erosion model, which provides a new calculation method to accurately predict the location and size of erosion. Lin et al. [17] considered the effects of gas–solid multiphase velocity and gas pressure and proposed a new model for predicting pipe erosion, which showed high accuracy in practical applications in the field. Hong et al. [18] studied the erosion of pipes with different structures. Zhao et al. [19] studied the erosion pattern of tandem elbows. Li [20] studied the numerical simulation of erosion wear of continuous elbows in different directions. Bilal [21] studied the erosion patterns and maximum erosion locations of elbows with different radii of curvature using a combination of CFD and experiments and concluded that the larger the radius of curvature, the lower the erosion rate. Zhu et al. [22] studied the effects of sand parameters, casing materials and formation temperature on the erosion rate of reservoir section casing during gas recovery using gas–solid two-phase flow erosion experiments and erosion simulation. CFD technology can simulate various flow patterns, from simple to complex, and various types of erosion models are highly flexible in predicting the erosion rate of pipes to fully and effectively consider the erosion mechanism.

Table 1 summarizes the studies conducted by some scholars in the field of erosion. In terms of experiments, many scholars have developed various erosion models based on experimental data. However, due to the complexity of erosion mechanisms and differences in experimental conditions, various types of erosion models are limited in terms of application conditions, which may lead to uncertainties when used under a wider range of conditions. In numerical simulations, there are large differences in the choice of erosion models and a lack of validation by experimental data. In this study, the maximum erosion rate of coiled tubing was studied using a combination of experimental data and numerical simulations. A suitable erosion model for coiled tubing under gas–solid two-phase flow condition is proposed, and a guidance scheme for reducing the maximum erosion rate of coiled tubing is presented.

Table 1. Summary of erosion studies.

Author	Method	Summary
Finnie Tilly Evans Tabakoff Hutchings Arabnejad	Experimental	Various erosion models based on different influencing factors were established
Edwards Shah Pandya Lin Hong Zhao Bilal Wang	Numerical simulation	The selection of erosion models varies widely

In this paper, an experimental device is established to simulate the erosion of full-size bends with different curvature radii, and different erosion models are compared with the experimental results using the CFD-DPM method. Based on the results, the erosion model is preferred. The relationship between the pipe bend radius, gas flow rate, solid-phase particle size and the maximum erosion rate of the pipe was investigated based on the selected erosion model. The results of this study can provide technical and theoretical support for the field application of coiled tubing.

2. Experiment

2.1. Experimental Device and Materials

Figure 1 is a schematic diagram of a full-size erosion simulator. A one-way injection pipe system was used in the experiment, and the air source was an air compressor. The gas flow provided by the air compressor is 50 m^3/h, and the gas flow rate during the experiment is 15 m/s. The air compressor outlet is sealed with a hose. The hose is installed with a pressure-regulating valve, a pressure monitor, a flow monitor and a sanding tank, which can control the sand rate. The end of the hose is closed to the coiled tubing. The end of the coiled tubing is connected to the sand collection device to collect sand and expel air. Figure 2 shows the erosion test module and photos.

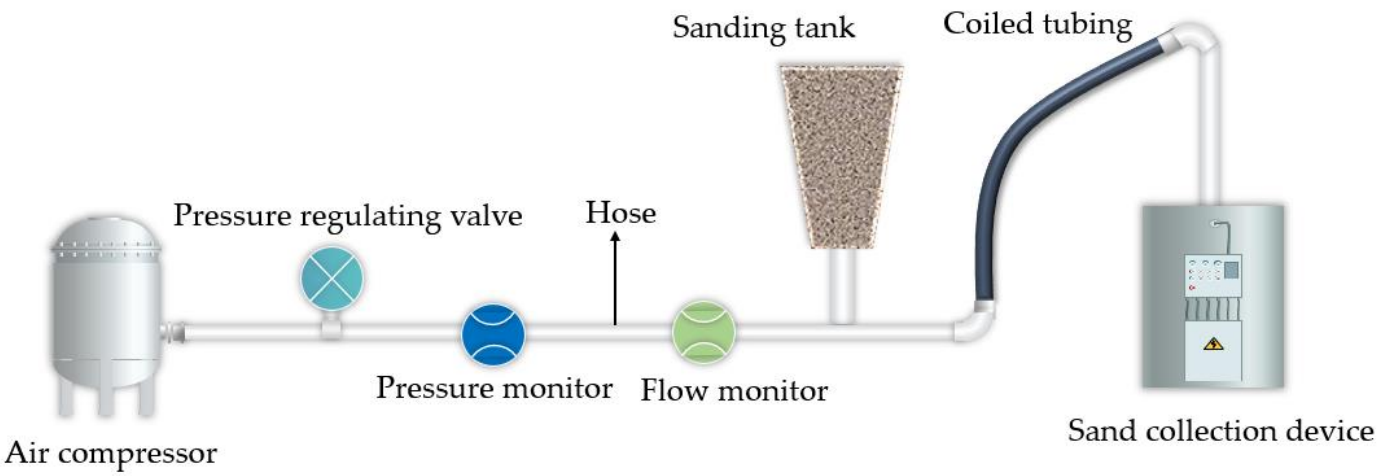

Figure 1. Schematic diagram of the full-size erosion simulator.

Quartz sand was used in the experiment, which was screened with a screen before the experiment. Figure 3 shows the screen and quartz sand used for sand screening. The sand particle size is 0.25 mm. The particle mass flow rate during the experiment was 3.00×10^{-4} kg/s.

The mass flow rate and head of the conveying system were calculated using the Bernoulli equation. The flow rate and head of the pump required in the experimental device were calculated as shown in Table 2. The transport liquid properties and operating conditions were used to determine the type of pump. In this experiment, we used a UHB-ZK-15-32 mortar pump (with a small control cabinet) produced by Shanghai Saitai Pump and Valve Co., Ltd., with a flow rate of 15 m^3/h and a lift of 30 m. The parameters of the pump are shown in Table 3. This pump is a single-stage, single-suction cantilever type centrifugal pump, with flow parts comprising a steel lining and ultra-high-molecular-weight polyethylene. The pump is resistant to corrosion and wear.

Before the experiment, the tube was cut into bisection samples to facilitate a parallel experiment. The internal diameter of the coiled tubing used in the erosion experiment was 3.3 cm; the material was N80 carbon steel; the pipe length was 1 m; and the curvature radii were 1.5 m, 3 m and 6 m. Each curvature radius had 4 bending pipes for the erosion experiment, and the erosion time was 15 h. Figure 4 shows the pipes used in the experiment.

(**a**) Air compressor (**b**) Sand screening operation

(**c**) Sanding tank (**d**) Flow measurement instrument

Figure 2. Photos of the experimental device.

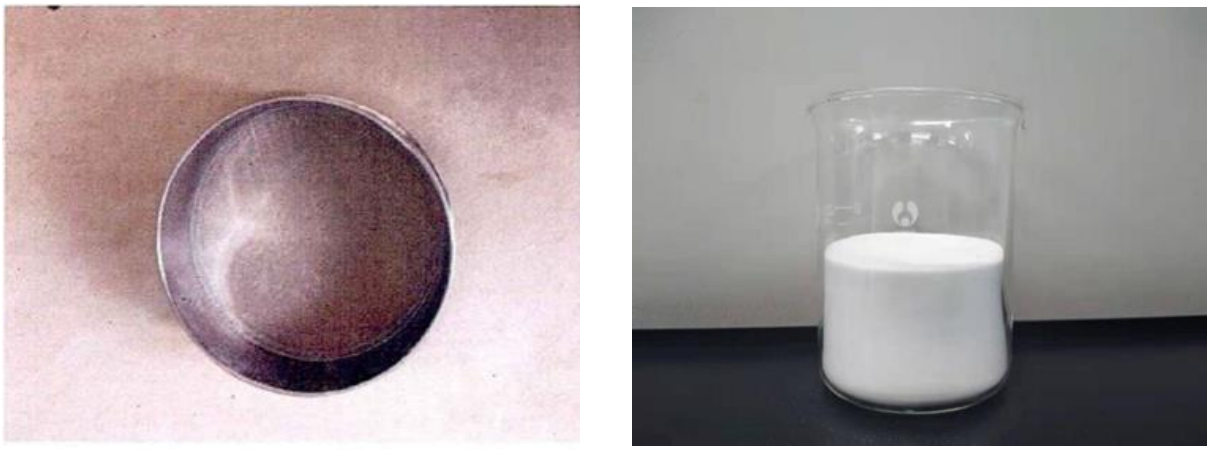

(**a**) screen (**b**) quartz sand

Figure 3. Screen and quartz sand used in the experiment.

Table 2. Flow rate and head required for the experiment.

Mass Flow Rate (kg/s)	Head (m)
6.25	30

Table 3. Performance parameters of the UHB-ZK-15-32 corrosion-resistant and wear-resistant mortar pump.

Flow Rate (m^3/s)	Head (m)	Rotational Speed (r/min)	Inlet and Outlet Diameter (m)	Equipped Motor (kW)	Shaft Power (kW)
15	32	2900	50 × 40	3.5	5.5

Figure 4. Coiled tubing with different radii of curvature.

After the experiment, a severely eroded section of CT with dimensions of 1 cm × 5 cm was cut and sampled. The cut sample was rinsed with distilled water, then cleaned with ethanol and allowed to dry. The prepared sample was scanned by an optical microscope, and a 3D profile was generated to determine the erosion degree of the CT inner wall.

2.2. Experimental Results

2.2.1. Macroscopic Damage Analysis

Erosion simulation experiments were conducted on 12 coiled tubing samples with 3 curvature radii (1.5 m, 3 m and 6 m). A total of more than 80 sections were analyzed, and the most obvious erosion marks at the inlet, middle and outlet were selected for comparison (Figure 5). Among the coiled tubing samples with 3 curvature radii, erosion damage occurred at the inner wall of the outer arc. The middle of the CT with a curvature radius of 1.5 m was marked by significant erosion (red dashed line box), while the other two curvature radii had relatively minor erosion damage.

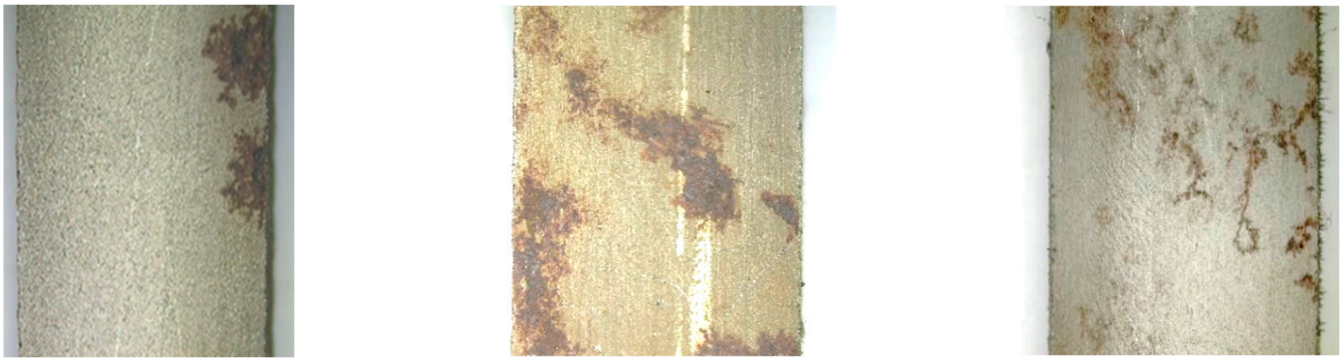

(**a**) Inlet (**b**) Central (**c**) Outlet

The macromorphology of erosion damage of the pipe wall with a curvature radius of 1.5 m.

(**d**) Inlet (**e**) Central (**f**) Outlet

The macromorphology of erosion damage of the pipe wall with a curvature radius of 3 m.

(**g**) Inlet (**h**) Central (**i**) Outlet

The macromorphology of erosion damage of the pipe wall with a curvature radius of 6 m.

Figure 5. Macroscopic erosion damage of pipes with different radii of curvature.

2.2.2. Microscopic Damage Analysis

In order to quantitatively analyze the damage degree (depth of erosion pits) before and after erosion, 3D laser confocal technology was used to quantitatively test and characterize the surface morphology of the tube wall surface. Figure 6 shows the surface morphology of the inlet, central and outlet parts of the CT without erosion at the position indicated in Figure 5. The maximum defect depth was 10.232 μm at the outlet.

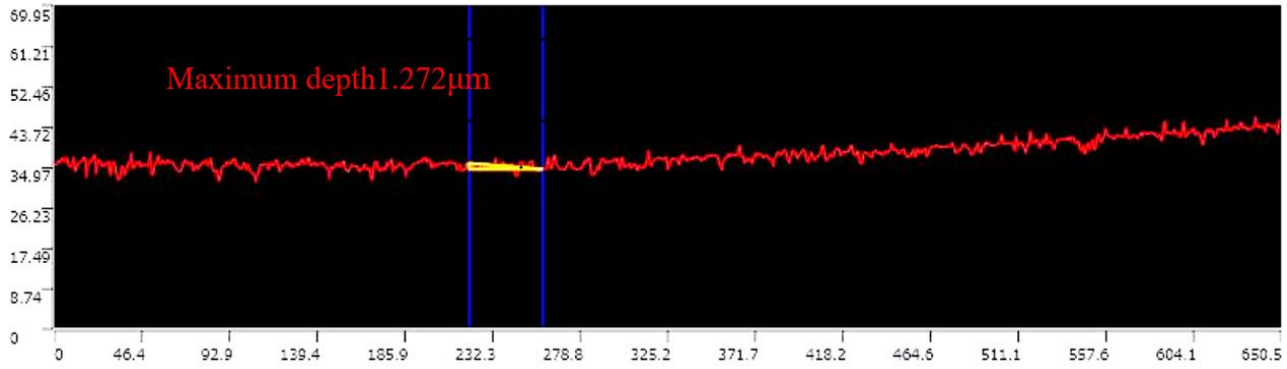

(**a**) Maximum depth of the inner wall at the inlet.

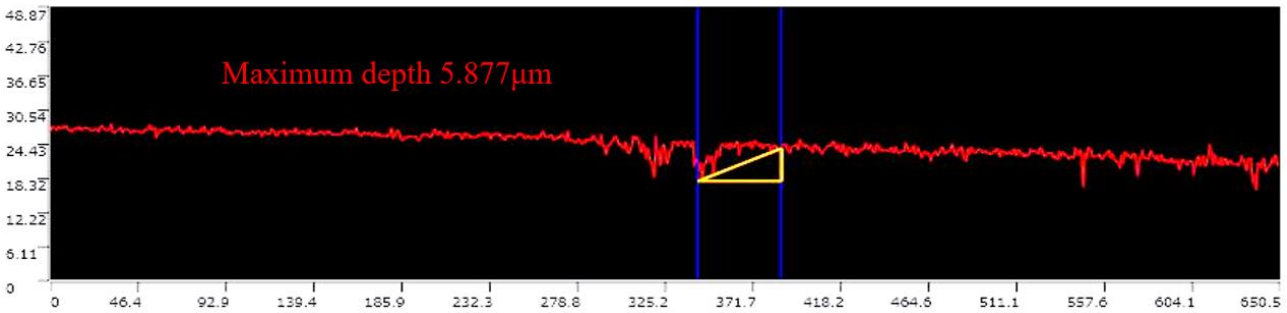

(**b**) Maximum depth of the inner wall at the central portion.

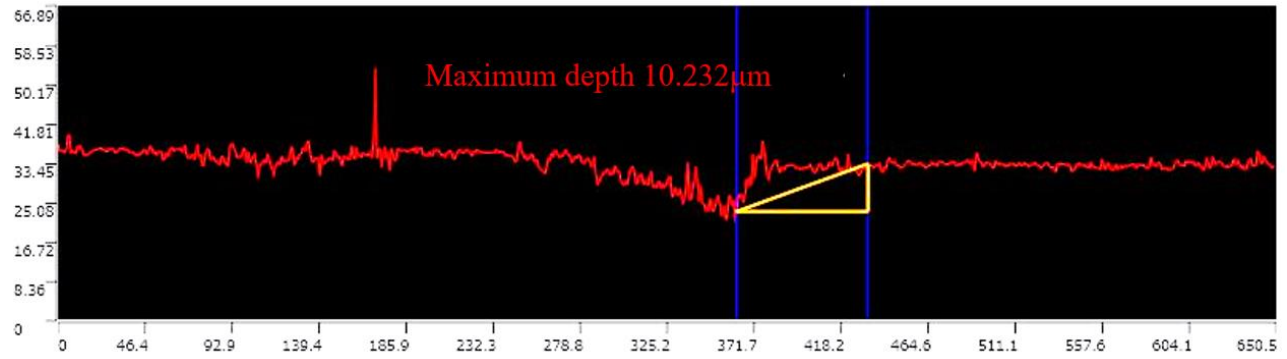

(**c**) Maximum depth of the inner wall at the outlet.

Figure 6. Microscopic profile of the inner wall of the pipe before erosion.

Figure 7 shows the quantitative analysis results of 3D morphology of erosion damage of CT with curvature radii of 1.5 m, 3.0 m and 6.0 m. The erosion damage degree in the central portion of CT with a curvature radius of 1.5 m is very serious, and the maximum erosion depth is 54.664 μm, which is about 3.3 times that of the maximum erosion depth of the pipe with a curvature radius of 6 m. The maximum depth of the erosion in the central portion of the CT with a curvature radius of 3.0 m is 37.108 μm, and the erosion damage is also relatively serious. The smaller the curvature radius, the more serious the erosion damage degree. The overall damage degree of coiled tubing with curvature radii of 1.5 m and 3.0 m is higher, while the damage degree of coiled tubing with a curvature radius of 6.0 m is minimal.

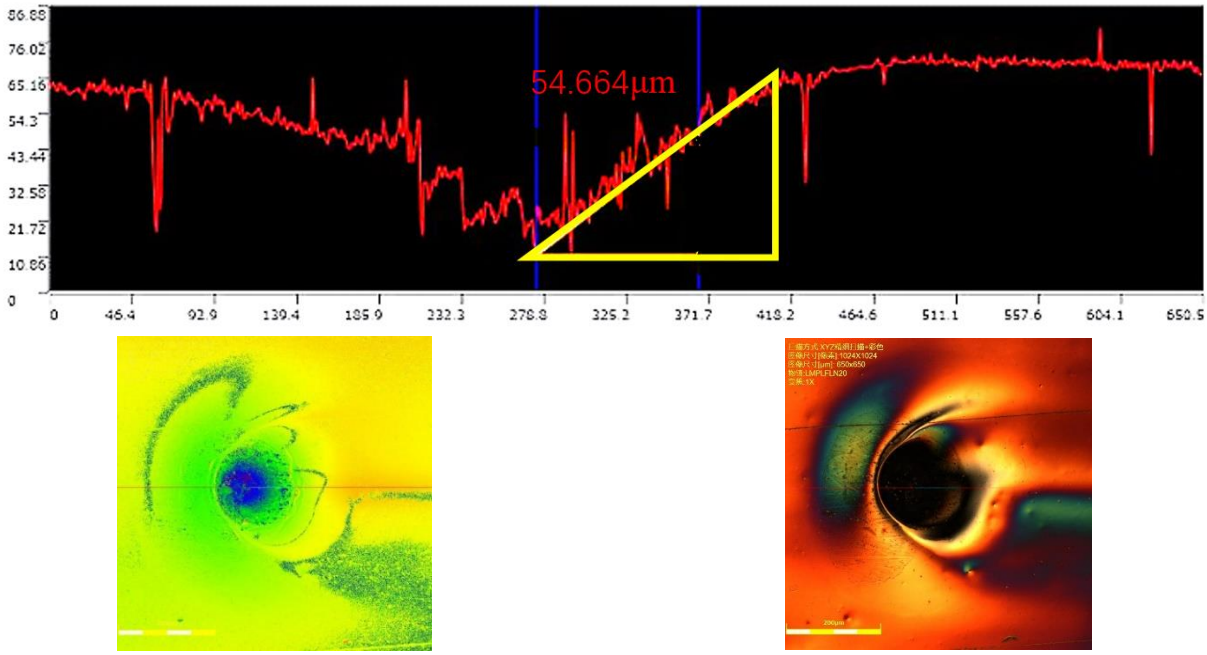

(**a**)

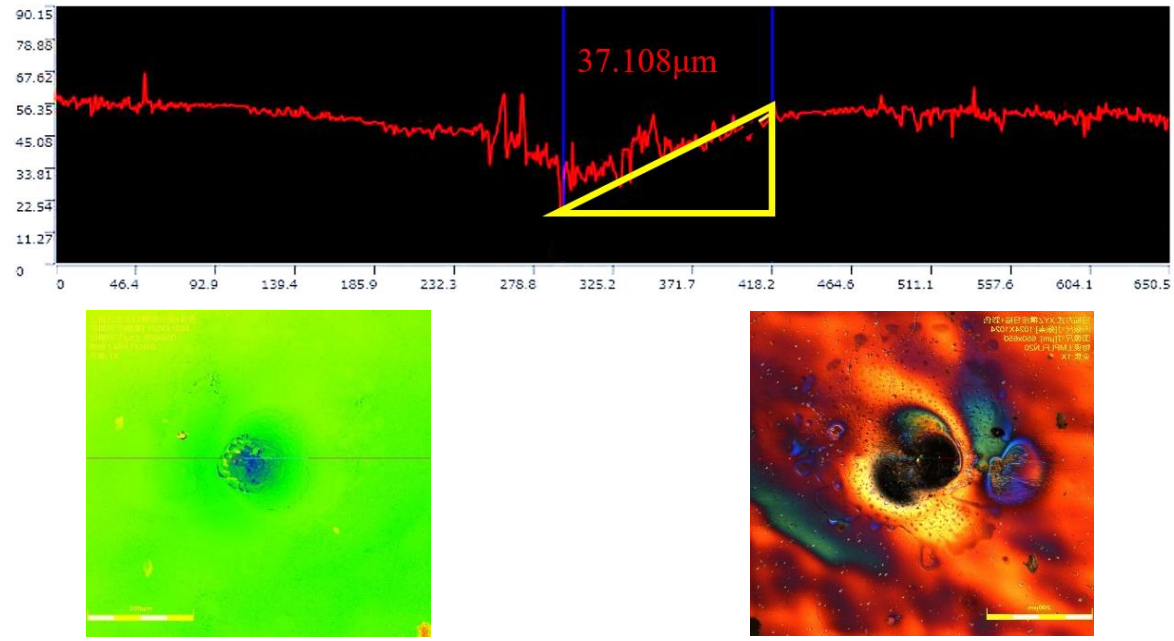

(**b**)

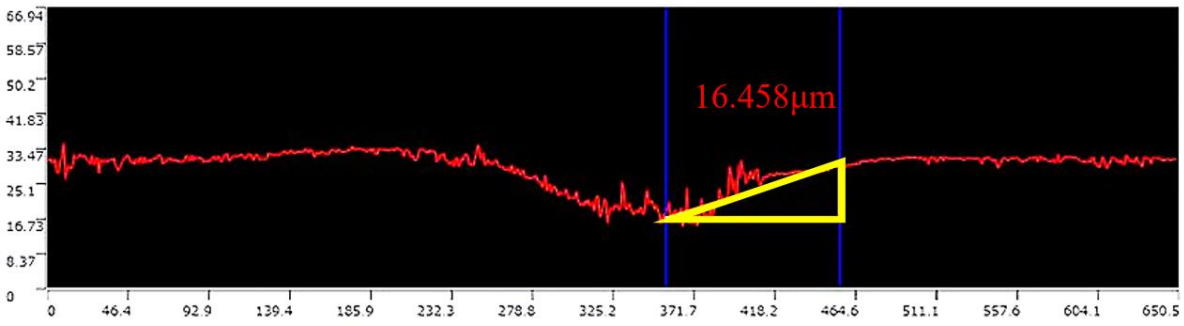

Figure 7. *Cont.*

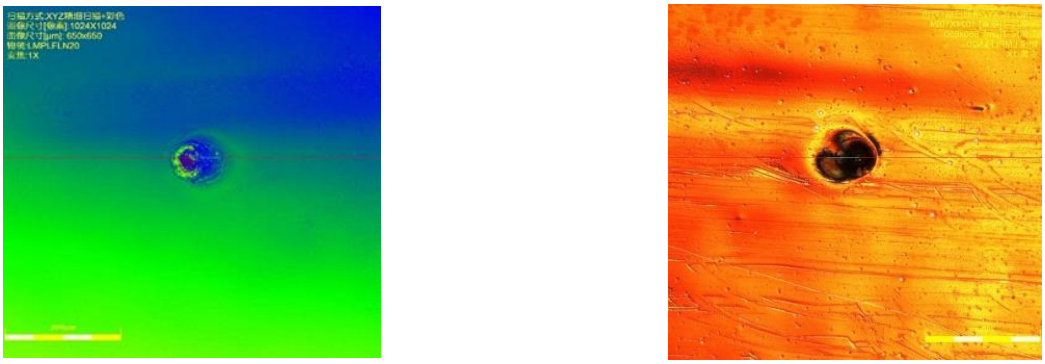

(**c**)

Figure 7. Three-dimensional profiles of the inner wall of pipes with different curvature radii after the erosion experiment. (**a**) Three-dimensional profile of the maximum erosion depth in the central portion of the pipe with a curvature radius of 1.5 m. (**b**) Three-dimensional profile of the maximum erosion depth in the central portion of the pipe with a curvature radius of 3 m. (**c**) Three-dimensional profile of the maximum erosion depth in the central portion of the pipe with a curvature radius of 6 m.

3. Numerical Simulation

In this study the erosion rate and the area prone to wear erosion of coiled tubing with different curvature radii were predicted based on the DPM erosion prediction model of the Euler–Lagrange algorithm. In the process of coiled tubing gas production, when sand-carrying gas quickly flows through the pipe, the flow field inside the gas production channel is a complex gas–solid two-phase flow field. The DPM model was used to conduct numerical simulations on the inside of the pipe. The continuous phase is natural gas, and the discrete phase is sand. The continuous phase flow field was calculated in the Eulerian coordinate system, and the discrete-phase trajectory equation was calculated in the Lagrangian coordinate system. The RNG k-ε model was adopted for the flow field in the device, and the gravitational acceleration was 9.8 m/s^2.

3.1. Theoretical Models and Control Equations

3.1.1. Continuous-Phase Equation

Gas flows in accordance with the law of conservation of mass, momentum and energy. As the influence of temperature on the gas pipe is small, the influence of temperature is ignored. The N-S equation is used to calculate the flow field. The mass equation and momentum equation are expressed as follows:

$$\frac{\partial \rho}{\partial t} + \nabla\left(\rho \vec{u}\right) = 0 \tag{1}$$

$$\frac{\partial}{\partial t}\left(\rho \vec{u}\right) + \nabla\left(\rho \vec{u}\vec{u}\right) = -\nabla p + \nabla \cdot \left(\overline{\overline{\tau}}\right) + \rho \vec{g} + \vec{S}_D \tag{2}$$

$$\overline{\overline{\tau}} = \mu\left[\left(\nabla \vec{u} + \nabla \vec{u}^T\right) - \frac{2}{3}\nabla \vec{u} I\right] \tag{3}$$

where ρ is the gas density (kg/m^3); $\vec{u}$ is the velocity vector (m/s), t is the time (s), p is the pressure (Pa), $\overline{\overline{\tau}}$ is the stress tensor, $\vec{g}$ is the gravitational acceleration (m/s^2), μ is the viscosity (Pa·s), I is the unit tensor and $\vec{S}_D$ is the source term.

3.1.2. Turbulence Model

Compared with the standard k-ε model, the RNG k-ε model has advantages in the flow field calculation and is more accurate, so the RNG k-ε turbulence model was chosen as the calculation model. The model equations are as follows.

$$\frac{\partial}{\partial t}(\rho k) + \frac{\partial}{\partial x_i}(\rho k u_i) = \frac{\partial}{\partial x_j}\left[\left(\mu + \frac{\mu_t}{\sigma_k}\right)\frac{\partial k}{\partial x_j}\right] + G_k + G_b - \rho\varepsilon - Y_M + S_k \quad (4)$$

$$\frac{\partial}{\partial t}(\rho \varepsilon) + \frac{\partial}{\partial x_i}(\rho \varepsilon u_i) = \frac{\partial}{\partial x_j}\left[\left(\mu + \frac{\mu_t}{\sigma_\varepsilon}\right)\frac{\partial \varepsilon}{\partial x_j}\right] + G_{1\varepsilon}\frac{\varepsilon}{k}G_k - G_{2\varepsilon}\rho\frac{\varepsilon^2}{k} + S_\varepsilon \quad (5)$$

$$\mu_t = \rho C_\mu \frac{k^2}{\varepsilon} \quad (6)$$

where k is turbulent kinetic energy (J); ε is the turbulent kinetic energy dissipation rate (J/s); u_i is the velocity of the fluid in direction I (m/s); x_i, x_j is the spatial coordinate component (mm); μ represents the dynamic viscosity of gas (Pa·s); μt is the eddy viscosity (Pa·s); G_k is the generation term of turbulent kinetic energy caused by average velocity; G_b is the generation term of turbulent kinetic energy (k) caused by buoyancy; Y_M is the wave energy generated by compressible turbulent kinetic energy; S_k and S_ε are customized dimensionless parameters; and $G_{1\varepsilon}$, $G_{2\varepsilon}$, C_μ, σ_k and σ_ε are empirical constants.

3.1.3. Discrete-Phase Model

The air flow in the curved pipe carries solid particles. The particle group is regarded as a discrete phase, and the discrete-phase model (DPM) is used to track the movement trajectory of solid particles in the air [23]. The motion of particles is simulated in a turbulent flow. The equation of motion is:

$$\frac{\mathrm{d}u_\mathrm{p}}{\mathrm{d}t} = F_D(u_g - u_\mathrm{p}) + \frac{g(\rho_p - \rho_g)}{\rho_p} + F_\mathrm{other} \quad (7)$$

$$F_D = \frac{18\mu}{\rho_p d_p^2}\frac{C_D Re}{24} \quad (8)$$

$$Re = \frac{\rho d_p |u_g - u_\mathrm{p}|}{\mu} \quad (9)$$

$$C_D = \frac{24}{R_e}\left(1 + b_1 Re^{b_2}\right) + \frac{b_3 Re}{b_4 + Re} \quad (10)$$

where ρ_p is particle density (kg/m^3); u_p is particle velocity (m/s); u_g is the airflow velocity (m/s); ρ_g is gas density (kg/m^3); $F_D(u_g - u_p)$ is the drag force on the particle (N); F_other is other forces on the particle (N); F_D is the drag force per unit mass due to the different velocities of gas–solid two phase flow (N); μ is fluid viscosity (Pa·s); Re is the particle Reynolds number; b_1, b_2 and b_3 are empirical constants; and C_D is the drag coefficient.

3.1.4. Particle Rebound Model

In a gas–solid two-phase flow field, particles contained in high-velocity gas impact the pipe wall and then leave at a certain angle of reflection. Forder et al. [24] proposed normal and tangential springback coefficients.

$$e_n = 0.998 - 0.78\alpha + 0.19\alpha^2 - 0.024\alpha^3 + 0.027\alpha^4 \quad (11)$$

$$e_t = 1 - 0.78\alpha + 0.84\alpha^2 - 0.21\alpha^3 + 0.028\alpha^4 - 0.022\alpha^5 \quad (12)$$

where e_n is the normal tangential coefficient, e_t is the tangential recovery coefficient and α is the particle impact angle.

3.1.5. Erosion Model

The flow field of sand-carrying gas and the erosion mechanism of curved pipes are complicated, involving many factors. There is no erosion model that takes all factors into account. Most erosion models are established based on empirical or semiempirical

formulas. In this study, four erosion models, i.e., the Generic [25], Finnie [26], DNV [27] and McLaury [28,29] models, were used to test the erosion rate of bent pipes; these models were evaluated and optimized based on the full-scale experimental data.

$$ER = \sum_{P=1}^{N_{particle}} \frac{m_p C(D_P) f(\alpha) v^{b(v)}}{A_{face}} \quad \text{Generic model} \quad (13)$$

$$E = kV_p{}^n f(\alpha) \quad f(\alpha) = \begin{cases} sin2\alpha - 3sin^2\alpha & (\alpha \le 18.5^\circ) \\ \frac{1}{3}cos^2\alpha & (\alpha > 18.5^\circ) \end{cases} \quad \text{Finnie model} \quad (14)$$

$$E = Kf(\alpha)V_p^n \quad f(\alpha) = \sum_{i=1}^{8} (-1)^{i+1} A^i \alpha^i \quad \text{DNV model} \quad (15)$$

$$E = AV_p^n f(\alpha) \quad A = FB_h{}^k \quad \text{McLaury model} \quad (16)$$

where ER is the erosion rate (kg/(m^2·s)), m_p is the particle mass flow rate (kg/s), $C(D_P)$ is the function of particle size, $f(\alpha)$ is the impact angle function, v is the particle impact velocity (m/s), $b(v)$ is the relative velocity function of particles, A_{face} is the wall area (m^2), E is the dimensionless erosion mass, k is a constant, V_p is particle velocity (m/s), $f(\alpha)$ is the impact function, α is the impact angle of particles, n is the velocity index, B_h is Brinell hardness (Mpa) and the remaining variables are empirical constants.

3.2. Model Optimization

CFD simulation was performed based on four types of erosion models for bending pipes with different curvatures. The geometric model used in CFD was consistent with the shape and size of the bending pipes used in the experiment. The entry and exit directions of the four models are consistent in the simulation calculation, and the results of the erosion simulation are shown in Figure 8. Each model shows that the erosion area of the bend is located on the inner wall of the outer bend of the pipe. As the radius of curvature decreases, the erosion area and the erosion rate of the pipe increase. Combining the motion trajectory of particles in curved pipes with different bend radii (Figure 9a) and the erosion rate graph, the area of maximum erosion rate gradually approaches the entrance as the bend radius decreases. The particles maintain their original motion and hit the inner wall of the outer arc of the bend. The particle concentration in this area is the highest (Figure 9b), resulting in severe erosion wear of the pipe.

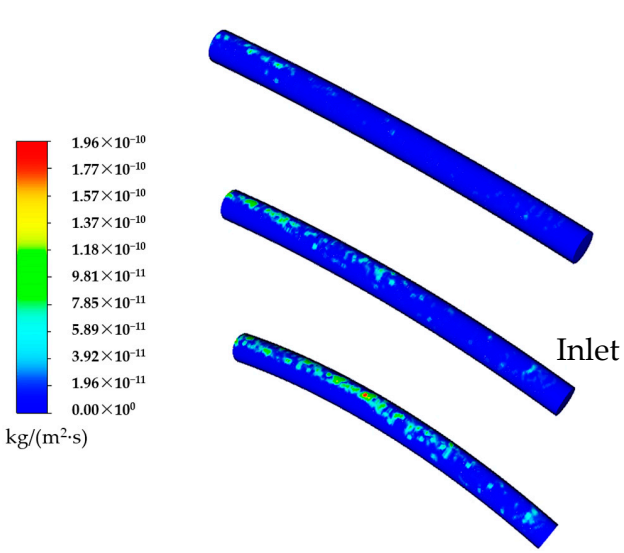

(**a**) Generic model

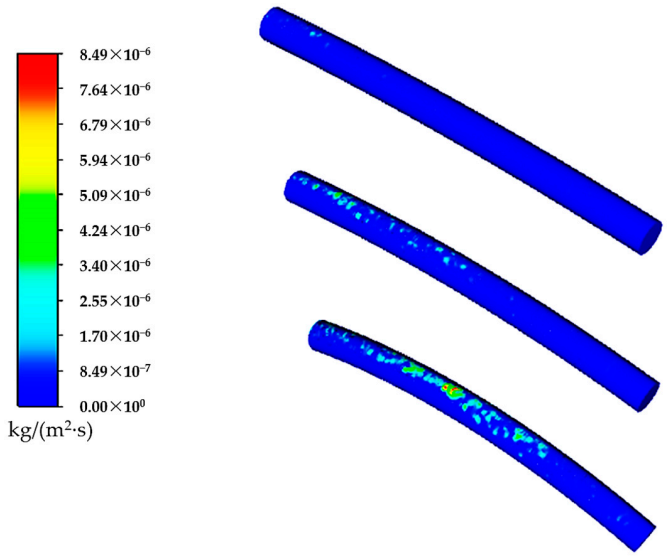

(**b**) Finnie model

Figure 8. *Cont.*

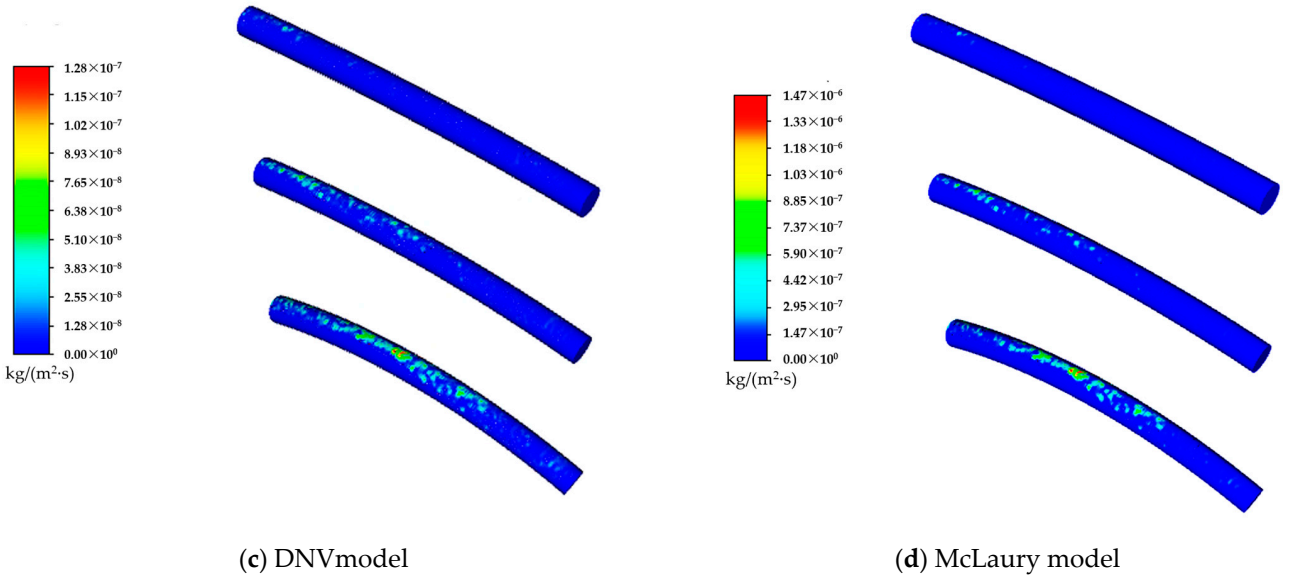

(**c**) DNVmodel (**d**) McLaury model

Figure 8. Erosion clouds under different erosion models.

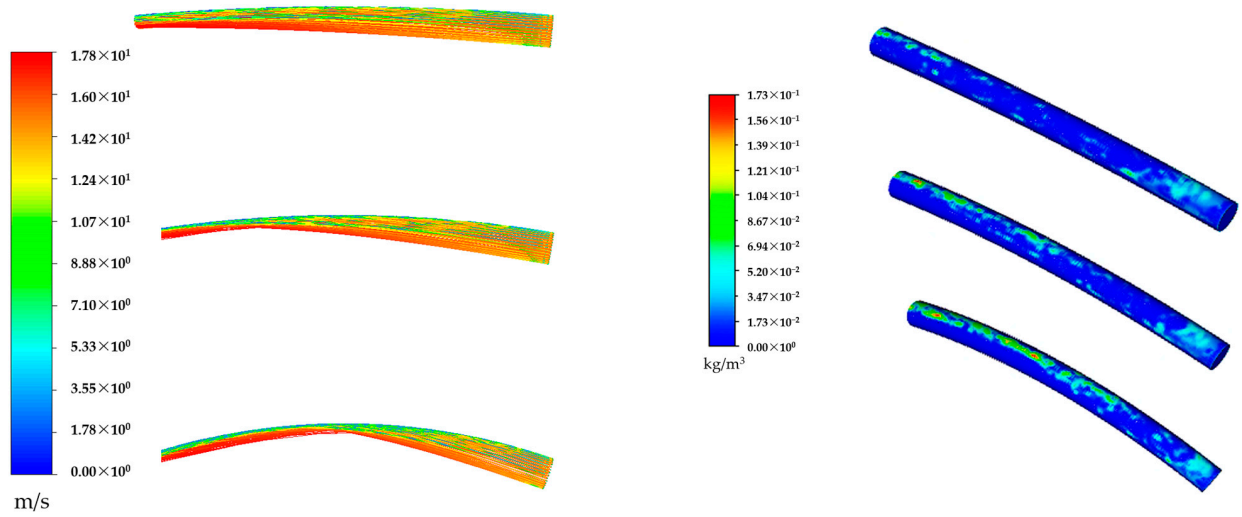

(**a**) Particle movement in the bend (**b**) Particle concentration cloud map

Figure 9. Particle movement and concentration distribution in the bend at different curvature radii.

The maximum erosion rate of each erosion model is different. The maximum erosion depth was calculated based on the maximum erosion rate of the four models and compared with the maximum erosion depth tested by the experiment, and the best model was selected. When the radius of curvature is 1.5 m, the maximum erosion rate of the Generic model is 1.96×10^{-10} kg/(m^{2}s). The maximum erosion wear rate of the DNV model is 1.28×10^{-7} kg/(m^{2}s), and that of the Mclaury model is 1.47×10^{-6} kg/(m^{2}s). The maximum erosion depth calculated by Generic, DNV and Mclaury models is quite different from the maximum erosion depth tested by the experiment, and the reliability is not good. The maximum depth of erosion of the pipe for the Finnie model calculated according to formula (17) with different radii of curvature is shown in Table 4. The variation rule of the erosion depth calculated by the model is basically consistent with the experimental results, and the average error of the erosion rate is 8.3%. Considering the system error and random error involved in the experimental measurement, the Finnie model has high accuracy in the simulation calculation of the erosion rate of gas–solid two-phase flow.

$$H = \frac{E_R t}{\rho} \tag{17}$$

where H is the maximum erosion depth calculated by simulation (m), E_R is the maximum erosion rate (kg/m^{2}s), t is time (s) and ρ is the pipe density (kg/m^3).

Table 4. Comparison between measured maximum erosion rate and simulated maximum erosion rate under different curvature radii.

Radius of Curvature (m)	Measured Value (μm)	Simulated Value (μm)	Error %
1.5	54.664	58.403	6.84
3	37.108	39.347	6.03
6	16.458	18.435	12.02

The Finnie model has a strong theory and does not rely too much on empirical parameters. This model can explain the law of plastic material erosion by rigid particles at low impact angle well. In this study, the Finnie model showed high accuracy in simulating erosion with a small pipe diameter and small pipe bending degree, and the conclusions drawn in this study were mutually verified with previous conclusions. Therefore, in engineering practice, the Finnie model can be used to predict the erosion rate and effective service life for small-diameter and low-bend pipes.

3.3. Sensitivity Analysis

Due to the high cost of coiled tubing, it is important to study its effective life when transporting high-velocity gas. The effective life of coiled tubing is greatly affected by the radius of curvature, gas velocity and solid particle size and can be artificially and effectively controlled. Therefore, it is of great significance in engineering practice to analyze the influence of these three factors on the erosion rate of the pipe and to prolong the effective service life.

The relationship between the erosion rate of the pipe and the radius of curvature was analyzed during model optimization. The radius of curvature has a great influence on the maximum erosion rate of the pipe. Figure 10 shows the relationship between the maximum erosion rate and the radius of curvature (particle mass flow rate is 3.00×10^{-4} kg/s, particle size is 250 μm, the gas flow rate is 15 m/s, the pipe diameter is 3.3 cm and the pipe length is 1 m). The smaller the radius of curvature of the pipe, the greater the degree of curvature, the more concentrated the area where the particles collide with the pipe wall and the greater the impact frequency per unit area. The angle of particle–wall collision also becomes larger, resulting in an increase in the maximum erosion rate of the pipe. The smaller the radius of curvature, the closer the particle strikes the pipe wall while maintaining its original motion toward the inlet (Figure 11), and the area of severe erosion and wear gradually shifts toward the inlet.

Among the many factors affecting the erosion rate of the pipe, the gas flow rate directly determines the impact velocity of the solid particles on the wall. Figure 12 shows the relationship between the maximum erosion rate of the pipe and the gas flow rate (particle mass flow rate is 3.00×10^{-4} kg/s, the particle size is 250 μm, the pipe curvature radius is 1.5 m, the inner diameter is 3.3 cm and the length is 1 m). The maximum erosion rate of the pipe increases with an increase in gas flow rate. On the one hand, the greater the gas flow rate, the greater the kinetic energy of particles. The greater the kinetic energy of particles, the greater the normal stress and shear stress of particles acting on the pipe wall. On the other hand, an increase in gas flow rate leads to an increase in the collision frequency between the particles and the pipe wall. The combined effect of these two aspects leads to an increase in the maximum erosion rate with an increase in the gas flow rate. The variation of gas flow rate has less effect on the distribution of the erosion area and only affects the erosion rate.

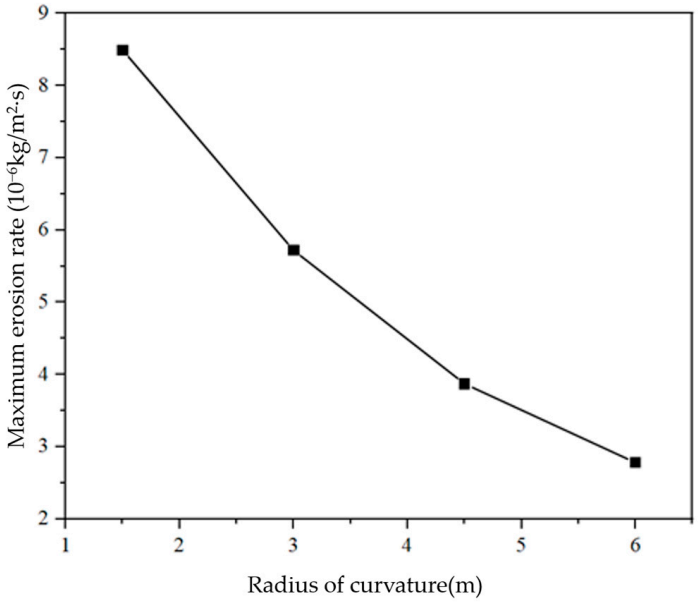

Figure 10. The relationship between the maximum erosion rate and the radius of curvature.

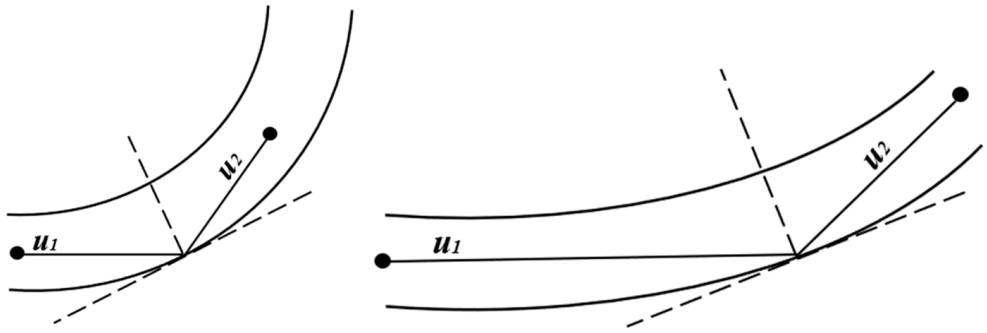

Figure 11. Schematic diagram of solid particle–wall collision at different radii of curvature.

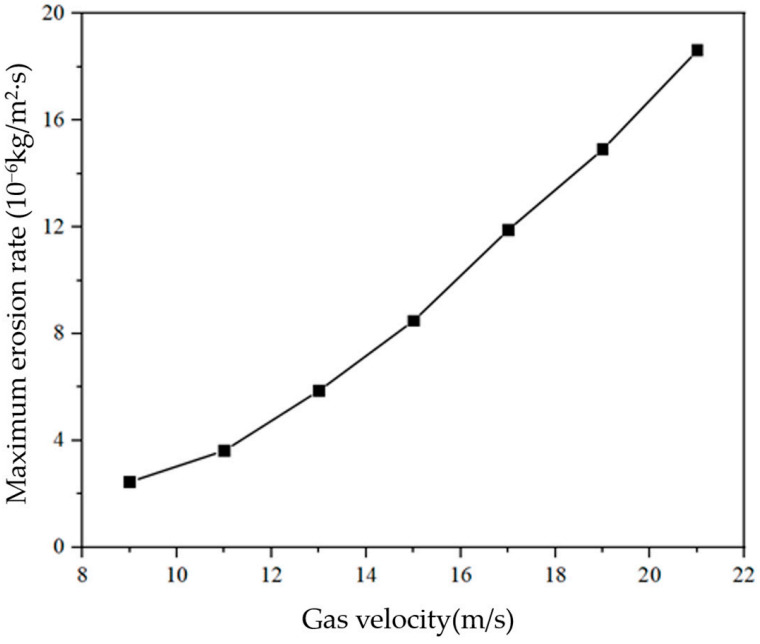

Figure 12. Relationship between maximum erosion rate and gas flow rate.

The particle size also affects the maximum erosion rate of the pipe. Figure 13 shows that with a radius of curvature of the pipe of 1.5 m, an inner diameter of 3.3 cm, a length of 1 m, a gas flow rate of 15 m/s and a mass flow rate of 3.00×10^{-4} kg/s), the maximum erosion rate is not simply positively correlated with the particle size. With an increase in particle size, the maximum erosion rate first increases, then decreases before stabilizing. When the particle size is less than 200 μm, the maximum erosion rate increases with the increase in particle size, while when the particle size is greater than 200 μm, the maximum erosion rate decreases with the increase in particle size before stabilizing. When the particle size is 200 μm, the erosion effect on the pipe is the largest, and the critical particle size is 200 μm. The critical particle size is the result of a variety of factors interacting with each other. When the particle size is small, its own mass is low, the kinetic energy is low and the impact of particles on the wall of the bend is weak, so the erosion rate is low. As the particle size increases, the particle mass and kinetic energy increase, the particle impact force per unit area on the inner wall of the bend reaches the maximum and the erosion rate reaches the maximum. The mass flow rate of particles is predictable, so as the particle size continues to increase, the number of particles decreases and the impact frequency of particles on the wall decreases; the larger the particle size, the greater the influence of gravity, and the trajectory of the particles produces a certain sink, which eventually leads to a lower erosion rate, eventually levelling off.

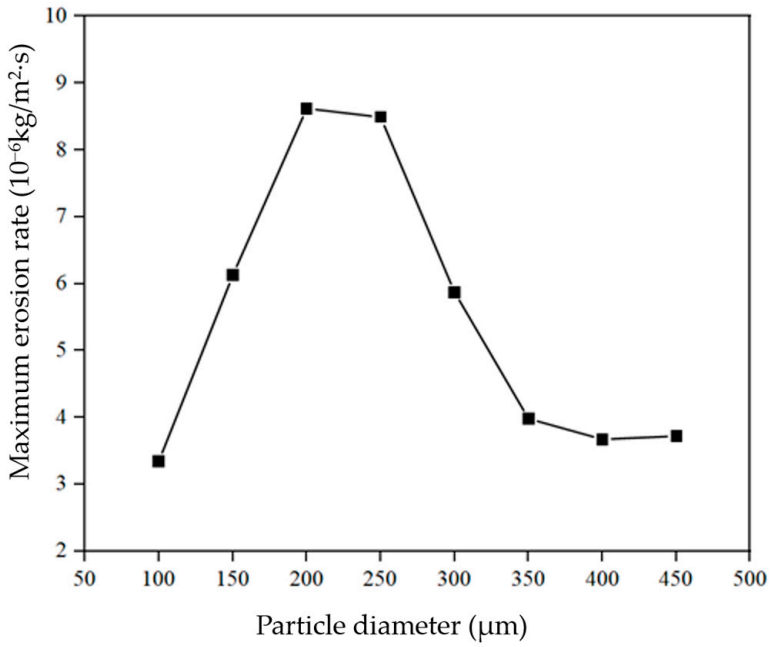

Figure 13. The relationship between maximum erosion rate and particle size.

4. Conclusions and Recommendations

In this paper, an experimental device for gas–solid erosion of a full-size pipe with different radii of curvature was constructed. The CFD-DPM method was used to simulate the erosion of the CT, and the erosion test data of the CT were compared with the erosion rates obtained from four erosion models to optimize the model. Sensitivity analysis of the factors affecting the erosion rate of the CT was also carried out using the preferred model. In this study, a combination of experimental and numerical simulations was used to propose a suitable erosion model for coiled tubing under gas–solid two-phase flow conditions. Through sensitivity analysis of the factors affecting the erosion rate, a guiding scheme was proposed to reduce the erosion rate and prolong the service life of the coiled tubing, which is significant for the use of coiled tubing in the field. The conclusions are as follows:

(1) For a pipe with small diameter and low bending degree, the Finnie model shows high accuracy in predicting the maximum erosion rate of the pipe by gas–solid two-phase flow, and the average error of the maximum erosion rate is 8.3%.
(2) The inner wall of the outer bend of the pipe is the most serious area for erosion and wear. As the radius of curvature of the pipe decreases, the location of the maximum erosion rate moves to the inlet, and the maximum erosion rate increases.
(3) The gas flow rate and the maximum erosion rate are positively correlated. The particle size and the maximum erosion rate show a complex relationship; with an increase in the particle size, the maximum erosion rate first increases, then decreases before stabilizing, with a critical particle size.
(4) In order to extend the effective life of coiled tubing, the maximum erosion rate can be reduced by controlling the production rate to reduce the gas flow rate in the tubing column and by adopting reasonable sand control methods for old wells. The maximum erosion rate can be reduced by adjusting the borehole trajectory to reduce the bending of the tubing column for new wells.

Author Contributions: Conceptualization, B.Z. and J.D.; methodology, J.D. and H.L.; software and validation, B.Z., H.L. and J.X.; writing—original draft preparation, B.Z., H.L. and G.W.; writing—review and editing, B.Z., W.Y. and J.X.; visualization, B.Z., K.W. and W.Y.; supervision, J.D. and F.L.; funding acquisition, J.D. and W.Y. All authors have read and agreed to the published version of the manuscript.

Funding: This research received no external funding.

Data Availability Statement: Not applicable.

Conflicts of Interest: The authors declare no conflict of interest.

Nomenclature

$\vec{u}$	Velocity vector, m/s
ρ	Gas density, kg/m^3
t	Time, s
p	Pressure, Pa
$\overline{\overline{\tau}}$	Stress tensor
$\vec{g}$	Gravitational acceleration, m/s^2
μ	Viscosity, Pa·s
I	Source term
k	Turbulent kinetic energy, J
ε	Turbulent kinetic energy dissipation rate, J/s
u_i	Velocity of the fluid in direction i, m/s
xi, xj	Spatial coordinate component, mm
μt	Eddy viscosity, Pa·s
ρ_p	Particle density, kg/m^3
u_p	Particle velocity, m/s
u_g	Airflow velocity, m/s
ρ_g	Gas density, kg/m^3
$F_D(u_g - u_p)$	Drag force on the particle, N
F_{other}	Other forces on the particle, N
CD	Drag coefficient
ER	Erosion rate, kg/(m^2·s)
m_p	Particle mass flow rate, kg/s
$C(D_P)$	Function of particle size
$f(\alpha)$	Impact angle function
$b(v)$	Relative velocity function of particles
A_{face}	Wall area, m^2

V_p	Particle velocity, m/s
α	Impact angle of particles
n	Velocity index
B_h	Brinell hardness, Mpa

References

1. Jiang, G.C.; Li, Y.Z.; He, Y.B.; Dong, T.F.; Sheng, K.M.; Sun, Z. Subsection and superposition method for reservoir formation damage evaluation of complex-structure wells. *Petrol. Sci.* **2023**, in press. [CrossRef]
2. Wang, Z.; Xu, Y.; Khan, N.; Zhu, C.; Gao, Y. Effects of the Surfactant, Polymer, and Crude Oil Properties on the Formation and Stabilization of Oil-Based Foam Liquid Films: Insights from the Microscale. *J. Mol. Liq.* **2023**, *373*, 121194. [CrossRef]
3. Reynolds, O. On the action of a blast of sand in cutting hard material. *Lond. Edinb. Dublin Philos. Mag. J. Sci.* **1873**, *46*, 337–343. [CrossRef]
4. Rayleigh, L. The sand blast. *Nature* **1914**, *93*, 188. [CrossRef]
5. Finnie, I. The mechanism of erosion of ductile metals. In Proceedings of the 3rd U.S. National Congress of Applied Mechanics, Providence, RI, USA, 11–14 June 1958; pp. 527–532.
6. Tilly, G.P. A two stage mechanism of ductile erosion. *Wear* **1973**, *23*, 87–96. [CrossRef]
7. Evans, A.G.; Gulden, M.E.; Rosenblatt, M. Impact damage in brittle materials in the elastic-plastic response regime. *Proc. R. Soc. Lond. A Math. Phys. Sci.* **1978**, *361*, 343–365.
8. Tabakoff, W.; Kotwal, R.; Hamed, A. Erosion study of different materials affected by coal ash particles. *Wear* **1979**, *52*, 161–173. [CrossRef]
9. Hutchings, I.M. A model for the erosion of metals by spherical particles at normal incidence. *Wear* **1981**, *70*, 269–281. [CrossRef]
10. Zeng, L.; Zhang, G.A.; Guo, X.P. Erosion–corrosion at different locations of X65 carbon steel elbow. *Corros. Sci.* **2014**, *85*, 318–330. [CrossRef]
11. Arabnejad, H.; Mansouri, A.; Shirazi, S.A.; McLaury, B.S. Abrasion erosion modeling in particulate flow. *Wear* **2017**, *376*, 1194–1199. [CrossRef]
12. Shahali, H.; Ghasemi, H.M.; Abedini, M. Contributions of corrosion and erosion in the erosion-corrosion of Sanicro28. *Mater. Chem. Phys.* **2019**, *233*, 366–377. [CrossRef]
13. Zhao, L.; Yan, Y.; Yan, X. A semi-empirical model for CO_2 erosion-corrosion of carbon steel pipelines in wet gas-solid flow. *J. Petrol. Sci. Eng.* **2021**, *196*, 107992. [CrossRef]
14. Edwards, J.K.; McLaury, B.S.; Shirazi, S.A. Modeling solid particle erosion in elbows and plugged tees. *J. Energy Resour. Technol.* **2001**, *123*, 277–284. [CrossRef]
15. Shah, S.N.; Jain, S. Coiled tubing erosion during hydraulic fracturing slurry flow. *Wear* **2008**, *264*, 279–290. [CrossRef]
16. Pandya, D.; Dennis, B.; Russell, R. An Improved Computational Fluid Dynamics (CFD) Model for Erosion Prediction in Oil and Gas Industry Applications. In Proceedings of the International Conference on Offshore Mechanics and Arctic Engineering, San Francisco, CA, USA, 8–13 June 2014.
17. Lin, N.; Lan, H.; Xu, Y.; Dong, S.; Barber, G. Effect of the gas–solid two-phase flow velocity on elbow erosion. *J. Nat. Gas Sci. Eng.* **2015**, *26*, 581–586. [CrossRef]
18. Hong, B.; Li, Y.; Li, X.; Ji, S.; Yu, Y.; Fan, D.; Qian, Y.; Gong, J. Numerical simulation of gas-solid two-phase erosion for elbow and tee pipe in gas field. *Energies* **2021**, *14*, 6609. [CrossRef]
19. Zhao, X.; Cao, X.; Xie, Z.; Cao, H.; Wu, C.; Bian, J. Numerical study on the particle erosion of elbows mounted in series in the gas-solid flow. *J. Nat. Gas Sci. Eng.* **2022**, *99*, 104423. [CrossRef]
20. Li, B.; Zeng, M.; Wang, Q. Numerical simulation of erosion wear for continuous elbows in different directions. *Energies* **2022**, *15*, 1901. [CrossRef]
21. Bilal, F.S.; Sedrez, T.A.; Shirazi, S.A. Experimental and CFD investigations of 45 and 90 degrees bends and various elbow curvature radii effects on solid particle erosion. *Wear* **2021**, *476*, 203646. [CrossRef]
22. Zhu, X.; Peng, P.; Jing, J.; Song, W. Research on casing erosion in reservoir section of gas storage wells sased on Gas-solid Two-phase flow. *Eng. Fail. Anal.* **2022**, *142*, 106688. [CrossRef]
23. Wang, K.; Li, X.; Wang, Y.; He, R. Numerical investigation of the erosion behavior in elbows of petroleum pipelines. *Powder Technol.* **2017**, *314*, 490–499. [CrossRef]
24. Forder, A.; Thew, M.; Harrison, D. A numerical investigation of solid particle erosion experienced within oilfield control valves. *Wear* **1998**, *216*, 184–193. [CrossRef]
25. Dennis, S.C.R.; Singh, S.N.; Ingham, D.B. The steady flow due to a rotating sphere at low and moderate Reynolds numbers. *J. Fluid Mech.* **1980**, *101*, 257–279. [CrossRef]
26. Finnie, I. Erosion of surfaces by solid particles. *Wear* **1960**, *3*, 87–103. [CrossRef]
27. Haugen, K.; Kvernvold, O.; Ronold, A.; Sandberg, R. Sand erosion of wear-resistant materials: Erosion in choke valves. *Wear* **1995**, *186*, 179–188. [CrossRef]

28. McLaury, B.S.; Shirazi, S.A. Generalization of API RP 14E for erosive service in multiphase production. In Proceedings of the SPE Annual Technical Conference and Exhibition, Houston, TX, USA, 3–6 October 1999.
29. McLaury, B.S.; Shirazi, S.A. An alternate method to API RP 14E for predicting solids erosion in multiphase flow. *J. Energy Resour. Technol.* **2000**, *122*, 115–122. [CrossRef]